Clocking Dissociative Above-Threshold Double Ionization of H_2 in a Multicycle Laser Pulse

Shengzhe Pan,[1] Wenbin Zhang,[1] Hui Li,[1] Chenxu Lu,[1] Weihua Zhang,[1] Qinying Ji,[1] Hanxiao Li,[1] Fenghao Sun,[1] Junjie Qiang,[1] Fei Chen,[1] Jihong Tong,[1] Lianrong Zhou,[1] Wenyu Jiang,[1] Xiaochun Gong,[1] Peifen Lu,[1] and Jian Wu[1,2,*]

[1]*State Key Laboratory of Precision Spectroscopy, East China Normal University, Shanghai 200241, China*
[2]*Collaborative Innovation Center of Extreme Optics, Shanxi University, Taiyuan, Shanxi 030006, China*

(Received 8 September 2020; accepted 21 January 2021; published 12 February 2021)

The dissociative above-threshold double ionization (ATDI) of H_2 in strong laser fields involves the sequential releasing of two electrons at specific instants with the stretching of the molecular bond. By mapping the releasing instants of two electrons to their emission directions in a multicycle polarization-skewed femtosecond laser pulse, we experimentally clock the dissociative ATDI of H_2 via distinct photon-number-resolved pathways, which are distinguished in the kinetic energy release spectrum of two protons measured in coincidence. The timings of the experimentally resolved dissociative ATDI pathways are in good accordance with the classical predictions. Our results verify the multiphoton scenario of the dissociative ATDI of H_2 in both time and energy fashion, strengthening the understanding of the strong-field phenomenon and providing a robust tool with a subcycle time resolution to clock abundant ultrafast dynamics of molecules.

DOI: 10.1103/PhysRevLett.126.063201

Exposed to a strong laser field, a molecule may absorb multiple photons more than necessary to overcome the double ionization threshold and break, accompanied by the releasing of two electrons, i.e., the dissociative above-threshold double ionization (ATDI) of molecules [1,2]. The exceeding photon energy is deposited into the ejected electrons and nuclear fragments. Beyond the sequentially or nonsequentially releasing dynamics of two electrons [1–7], the abundant structures of the measured kinetic energy release (KER) spectrum of the nuclear fragments allow us to understand the dissociative ATDI of molecules in the scenarios of charge-resonance-enhanced ionization [8,9] and above-threshold Coulomb explosion [10,11], respectively, in tunneling and multiphoton regimes. The former, assisted by the boosted tunneling of the localized electron around the critical internuclear distance, has clarified the generally observed much smaller KER of the nuclear fragments than the one expected from a direct Coulomb explosion of the multiply ionized molecules. The latter, characterized with multipeak KER spectrum, provides access to photon-number-resolved pathways, which is straightforward to be understood in the multiphoton scenario [10,11] and allows us to count the number of absorbed photons.

Although the KER spectrum has provided abundant details of the dissociative ATDI process, a time-resolved measurement visualizing the real-time dynamics will surely deepen our understanding of the observed phenomena and verify the multiphoton scenario. Intuitively, by absorbing different numbers of photons at different internuclear distances, different timings are expected for different pathways. It was predicted that a pump-probe measurement with few-cycle laser pulses (less than 5 fs) would allow one to time resolve various pathways in the dissociative ATDI of H_2 [12], which, however, has not been experimentally reported so far. In analogy to the angular streaking technique with a circularly polarized near-infrared laser pulse [13–17], the ultrafast stopwatch using a multicycle polarization-skewed (PS) laser pulse was verified to be robust with a subcycle time resolution (since electrons emitted in adjacent half-cycles end with opposite momenta) to pump probe the ultrafast dynamics of the molecules [18].

In this Letter, we experimentally clock the dissociative ATDI of H_2 using the ultrafast stopwatch of a multicycle PS laser pulse by measuring two electrons and two protons ejected from a doubly ionized H_2 in coincidence. As illustrated in Fig. 1(a), the instants of the first and second ionization steps are encoded in the emission directions of two released electrons, forming an X-shaped momentum distribution. Their crossing angle records the time interval between two ionization steps. Meanwhile, the multipeak KER spectrum of two protons allows us to identify different dissociation pathways. By investigating the nuclear KER spectrum and the electron emission directions in a PS laser pulse, we resolve the timings of distinct dissociative ATDI pathways of H_2 where the molecular ion dissociates along different potential energy curves by absorbing different numbers of photons.

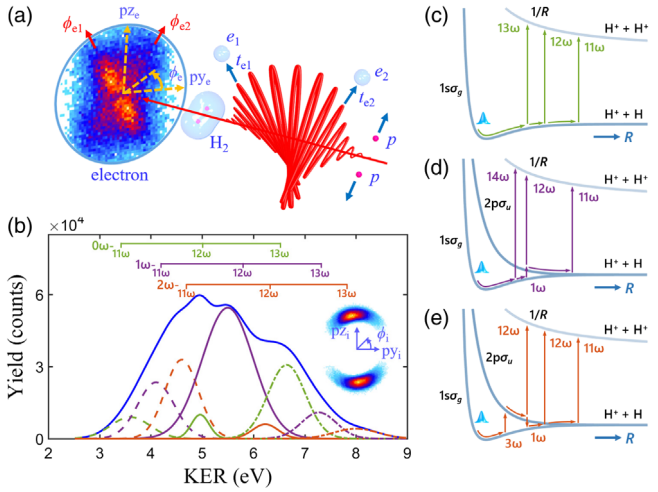

FIG. 1. (a) Schematic illustration of the ultrafast stopwatch using a multicycle PS laser pulse to clock the dissociative ATDI of H_2. Two electrons sequentially released at different instants are angularly streaked to different emission directions by the PS laser pulse, leading to an X-shaped photoelectron momentum distribution. (b) The measured KER spectrum and momentum distribution (inset) of two protons in dissociative ATDI of H_2 driven by a PS laser pulse. The vertical ticks on the horizontal lines indicate the classically predicted KERs of different dissociation pathways. (c)–(e) Classical propagation of the nuclear wave packet of the first ionization created H_2^+ on different potential energy curves until the second ionization of the molecule to transit to the $1/R$ curve of the (c) direct, (d) one-photon, and (e) net-two-photon pathways of the dissociative ATDI of H_2.

Experimentally, the PS laser pulse is constructed by propagating a linearly polarized femtosecond laser pulse (28 fs, 790 nm) through a multiorder wave plate (MOWP) in conjunction with a Berek compensator [18,19]. The incident linearly polarized laser pulse [polarized along the z axis shown in Fig. 1(a)] is converted into two orthogonally polarized subpulses polarized along the fast and slow axes of the MOWP at 135° and 45° with respect to the y axis, respectively. The polarization of the PS laser field rotates from 135° (315°) to 45° (225°) in the y-z plane given by the orientation of the fast and slow axes of the MOWP. In our experiment, the time lag between two orthogonally polarized components is set to be $10T$, where $T = 2.6$ fs is the optical cycle of the incident near-infrared light. The peak intensity of the incident linearly polarized laser pulse in the interaction region was measured to be $I_0 = 5 \times 10^{14}$ W/cm^2, which corresponds to a peak intensity of 1.3×10^{14} W/cm^2 of the here-constructed PS pulse. By focusing the PS pulse onto a supersonic H_2 beam in an ultrahigh vacuum chamber of a cold target recoil ion momentum spectrometer [20,21], two protons and two electrons ejected from a doubly ionized H_2 are detected in coincidence.

In the following, we first identify different photon-number-resolved pathways in the KER spectrum and then clock the dynamics of various pathways using the ultrafast stopwatch of the PS laser pulse. The blue curve in Fig. 1(b) displays the measured KER spectrum of two protons from the dissociative ATDI of H_2. The corresponding momentum distribution of the protons in the polarization plane of the PS laser pulse is shown in the inset on the right. Here, the dissociative ATDI events are selected by considering the momentum conservation of two electrons and two protons, i.e.,$|pz_{e1} + pz_{e2} + pz_{i1} + pz_{i2}| < 0.5$ a.u., along the time-of-flight direction of the spectrometer. The multipeak structure of the KER spectrum corresponds to various pathways of the dissociative ATDI of H_2 by absorbing different numbers of photons, whose probabilities are numerically fitted using multiple Gaussian functions shown with curves of different colors below the blue curve in Fig. 1(b). These Gaussian functions are initialized with KER peaks classically predicted as follows and shared a common initial width. The numerical fitting returns nine photon-number-resolved pathways, which can be divided into three groups separated with photon energies and will be discussed in the following. The here-identified photon-number-resolved pathways are latterly confirmed by the visualized timings of the corresponding pathways.

By assuming the first ionization of H_2 at the equilibrium internuclear distance (∼1.4 a.u.), the subsequent bond stretching and ionization of the newborn H_2^+ along different potential energy curves can be divided into three groups. Here the photon-coupled resonant transitions between different potential energy curves at various internuclear distances are included during the stretching of the molecular ion. Although the ponderomotive or ac-Stark shift induced by the ultrashort laser pulse alters the kinetic energy of the emitted photoelectron, it has much less effect on the nuclear wave packet for its much heavier mass and relatively slow dynamics. It is actually negligible for a fast oscillating laser field with a central wavelength at 790 nm [22]. Here we hence use the field-free potential curves in our simplified model to simulate the propagation of the nuclear wave packet (NWP) [18,23,24]. An initial kinetic energy is assumed for the NWP of H_2^+ to account for the population at different vibrational states upon the first ionization of H_2. The three groups of pathways with distinct initial kinetic energies are following: (1) Direct pathway (0ω), as guided by the green arrows in Fig. 1(c), the NWP of H_2^+ with an initial kinetic energy of 1.9 eV (near the dissociation threshold of the $1s\sigma_g$ state) outward propagates along the $1s\sigma_g$ curve. The stretching H_2^+ may absorb 13, 12, and 11 photons at $R = 4.7$, 5.9, and 8.0 a.u. and transit to the $1/R$ curve of the Coulomb explosion by releasing the second electron. The corresponding KERs of two ejected protons along the $1/R$ curve and the time intervals (in the brackets) between two ionization steps are thus classically predicted to be 6.5 (6.9), 5.0 (11.3), and 3.4 eV (29.1 fs), respectively, which are labeled as 0ω-13ω, 0ω-12ω, and 0ω-11ω pathways. Here ω denotes the carrier

frequency of the incident PS laser pulse. (2) One-photon pathway (1ω), as guided by the violet arrows in Fig. 1(d), the H_2^+ with an initial kinetic energy of 1.2 eV of the NWP (composed of vibrational states centered at $v = 9$) stretching along the $1s\sigma_g$ curve may absorb 1ω at $R = 4.7$ a.u. and transit to the excited state of $2p\sigma_u$. It can afterward absorb 12ω and transit to the $1/R$ curve at $R = 4.7$ a.u. or further stretch along the $2p\sigma_u$ curve and absorb 11ω to transit to the $1/R$ curve at $R = 7.7$ a.u. by releasing the second electron, which are respectively labeled as the 1ω-12ω and 1ω-11ω pathways. There is also a probability for the H_2^+ to absorb 14ω at $R = 4.0$ a.u., where the overall number of absorbed photons is similar to the previous two pathways and which is thus labeled as the 1ω-13ω pathway. The predicted KERs and time intervals between two ionization steps are 7.3 (6.0), 5.8 (11.1), and 4.2 eV (25.6 fs), respectively, for the 1ω-13ω, 1ω-12ω, and 1ω-11ω pathways. (3) Net-two-photon pathway (2ω), as guided by the orange arrows in Fig. 1(e), the H_2^+ with an initial kinetic energy of 0.1 eV of the NWP (composed of vibrational states centered at $v = 3$) stretching on the $1s\sigma_g$ curve absorbs 3ω at $R = 3.3$ a.u. and transits to the $2p\sigma_u$ curve. The H_2^+ may afterward absorb 12ω and transit to $1/R$ curve at $R = 4.7$ a.u. by releasing the second electron, or emit 1ω at $R = 4.7$ a.u. to transit back to the $1s\sigma_g$ state, after which the H_2^+ further absorbs 12ω and 11ω at $R = 5.9$ and 8.0 a.u. upon the releasing of the second electron, respectively. The predicted KERs and time intervals between two ionization steps are 7.8 (12.5), 6.3 (14.9), and 4.7 eV (19.8 fs), respectively, for the 2ω-13ω, 2ω-12ω, and 2ω-11ω pathways.

After having identified distinct pathways in the KER spectrum, we will now clock various ATDI pathways of H_2 using the ultrafast stopwatch of a PS pulse. By gating the KER spectrum of the protons within ± 0.2 eV around the peaks of different pathways, we obtain the corresponding momentum (or angular) distributions of two released electrons, from which we can retrieve the time intervals between two ionization steps. We note that the KER region (from 3.2 to 3.6 eV) is gated for the 0ω-11ω pathway to reduce the mixture with other pathways, and relatively large KER gate widths of 0.5 eV (from 7.2 to 7.7 eV) for the 1ω-13ω pathway and 0.8 eV (from 7.7 to 8.5 eV) for the 2ω-13ω pathway are applied to have sufficient events to retrieve the corresponding time intervals. As an example, here we use the 0ω-11ω, 1ω-11ω, and 2ω-11ω pathways to demonstrate the validity and self-consistency of the strategy. For these three pathways, the first ionization created H_2^+ stretching along different potential energy curves will experience different time intervals before the second ionization step occurring at almost the same internuclear distance.

Figures 2(a)–2(c) display the electron momentum distributions of the 0ω-11ω, 1ω-11ω, and 2ω-11ω pathways by gating the KERs of the two protons within the ranges of $3.2 < \mathrm{KER} < 3.6$, $3.9 < \mathrm{KER} < 4.3$, and $4.4 < \mathrm{KER} < 4.8$ eV, respectively. Excited by a multicycle linearly or circularly polarized laser pulse, two electrons released from the double ionization are difficult to distinguish from each other for their similar momentum distributions, while two electrons released at different instants in a multicycle PS laser pulse sequentially emit

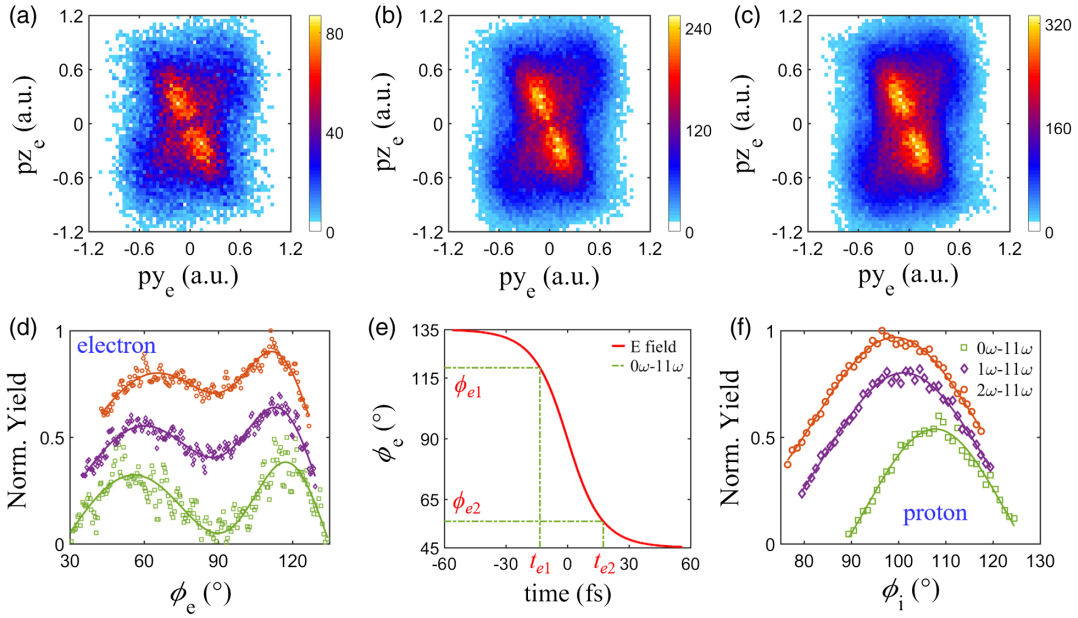

FIG. 2. (a)–(c) Measured momentum distributions of two electrons of the (a) 0ω-11ω, (b) 1ω-11ω, and (c) 2ω-11ω pathways. (d),(f) The corresponding angular distributions of the (d) electrons and (f) protons are plotted for the 0ω-11ω (green), 1ω-11ω (violet), and 2ω-11ω (orange) pathways, respectively. (e) The mapping function of the releasing instants of the electrons to the emission directions relating to the spatiotemporal profile of the multicycle PS laser pulse.

to distinct directions, leading to the X-shaped structure. The crossing angle of the X-shaped electron momentum distribution encodes the time interval between two ionization steps of the dissociative ATDI of H_2, i.e., $\Delta\varphi_e(=|\varphi_{e2}-\varphi_{e1}|)\sim\Delta t(=t_{e2}-t_{e1})$, where φ_{ei}, t_{ei} $(i=1,2)$ are the emission directions and releasing instants of the first and second electrons, respectively. We note that no diagonal distribution with a slope of -1 in the electron-electron 2D correlation energy map is observed, which agrees with the fact that two electrons are sequentially emitted in the here-observed dissociative ATDI of H_2.

To quantitatively extract the time intervals, as shown in Fig. 2(d), the momentum distributions of two electrons are converted into the angular distributions by integrating over the region of $0.25 < py^2 + pz^2 < 1$ a.u. in the polarization plane. The 1D angular distributions of two electrons are numerically fitted using two Gaussian functions to obtain the most probable emission directions. For an example of the 0ω-11ω pathway, two electrons mostly emit to $\varphi_{e1} = 119.2°$ and $\varphi_{e2} = 55.9°$, indicating that the two electrons are, respectively, released in the leading and lagging edges of the PS laser pulse. The width of the second emitted electron is always larger than the first one due to the dispersion of the NWP as its propagation on the potential energy curves compared to its well-localized distribution at the first ionization instant. Figure 2(e) displays the mapping function of the releasing instant of the electron to its emission direction relating to the spatiotemporal profile of the PS laser pulse (for more details on the mapping function, one can refer to [18]). We define the center of the PS laser pulse as $t = 0$, and the leading (lagging) edge of the laser pulse has a negative (positive) time. As guided by the vertical and horizontal dash-dotted green lines, the retrieved releasing instants of two electrons are $t_{e1} = -13.4$ and $t_{e2} = 17.5$ fs, resulting in a time interval between two ionization steps of $\Delta t = 30.9$ fs. This is in accordance with the classically predicted time interval of 29.1 fs for the 0ω-11ω pathway. For the 1ω-11ω and 2ω-11ω pathways, as shown in Figs. 2(b)–2(d), the crossing angles between emission directions of two electrons are smaller than the one of the 0ω-11ω pathway, indicating shorter time intervals between two ionization steps, which are measured to be 25.6 and 21.6 fs, respectively. The experimentally measured time interval of each pathway clearly differs from the neighboring ones, indicating that there is only one main pathway in the gated KER range of the nuclear fragments.

Figure 3(a) summarizes the emission directions of the two electrons of seven pronounced pathways measured in the experiment, where different pathways are coded with distinct colors. Since the KER distributions of the 0ω-12ω and 2ω-12ω pathways are highly overlapped with other pathways, and thus are hard to be obviously extracted by gating the KER spectrum, we cannot unambiguously obtain their timings from our experimental data. The hollow

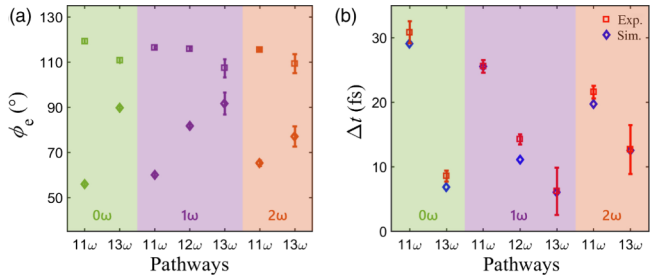

FIG. 3. (a) The measured most probable emission directions of the first (hollow squares) and the second (hollow diamonds) electrons of different pathways. (b) The measured (hollow squares) and classically predicted (hollow diamonds) time intervals of two ionization steps of different pathways.

squares and diamonds in Fig. 3(a) denote the emission directions of the first and the second electrons, respectively. Although the emission directions of the first electron (hollow squares) are more or less the same around $\varphi_{e1} = 110°$, the second electron emits to different directions (hollow diamonds) for different pathways varying from $\varphi_{e2} = 55°$ to 90°. Therefore, as shown in Fig. 3(b), the time intervals between two ionization steps, i.e., Δt, are distinct for various pathways. For instance, the Δt of the 0ω-13ω pathway is 8.6 fs, which is much shorter than the one of the 0ω-11ω pathway (30.9 fs), in agreement with the fact that the second ionization step occurs at a shorter internuclear distance at $R = 4.7$ a.u. for the 0ω-13ω pathway than $R = 8.0$ a.u. for the 0ω-11ω pathway. As summarized in Fig. 3(b), the experimentally resolved time intervals between two ionization steps (hollow red squares) of the 0ω-11ω, 0ω-13ω, 1ω-11ω, 1ω-12ω, 1ω-13ω, 2ω-11ω, and 2ω-13ω pathways are 30.9 (29.1), 8.6 (6.9), 25.6 (25.6), 14.3 (11.1), 6.2 (6.0), 21.6 (19.8), and 12.7 fs (12.5 fs), respectively, which is in agreement with the classically predicted ones [in the brackets, hollow blue diamonds in Fig. 3(b)]. The tiny discrepancy between the experimental and the predicted results is mainly due to the simplification of the classical model. Thus, the energy-and-time fashion agreement, i.e., the observed KERs of the nuclear fragments and the time intervals between two ionization steps retrieved from the electron angular distributions, confirms the assignment of the photon-number-resolved pathways and further the multiphoton scenario.

The experimentally resolved releasing instants of two electrons of different pathways are also in accordance with the observed angular distributions of the correlated protons. As shown in Fig. 2(f), the green, violet, and orange symbols (fitting curves) denote the proton angular distributions of 0ω-11ω, 1ω-11ω, and 2ω-11ω pathways, respectively. Since the maximal electric field is pointing to the z axis, a virtual double ionization process with zero time interval between the single and double ionization steps should happen at the peak of the electric field, resulting in the most probable emission direction of both protons and electrons

along the z axis, i.e., $\varphi_i = \varphi_e = 90°$. For an actual double ionization process in the PS laser pulse, the proton emission direction is always greater than 90°, i.e., $\varphi_i > 90°$, because the orientation of the molecular axis is preselected in the first ionization step, which is favored for molecules orientated parallel to the polarization direction of the leading edge. Thus the shift of the observed proton emission directions to a smaller angle along the rotation of the polarization of the PS pulse can reflect the time delay of the second ionization step with respect to the first one. The observed relative shifts of the proton emission directions of the 0ω-11ω, 1ω-11ω, and 2ω-11ω pathways, as shown in Fig. 2(f), qualitatively verify the retrieved time intervals between two ionization steps from the corresponding angular distributions of two electrons.

In conclusion, we demonstrate that the stopwatch of a multicycle PS laser pulse can be utilized to clock the photon-number-resolved dissociative ATDI of H_2. The instants of the first and the second ionization steps can be retrieved from the X-shaped momentum distributions of two electrons measured in coincidence with two protons ejected from a doubly ionized H_2 molecule. The good agreement with the classical predictions confirms the validity of the strategy and deepens our understanding of the multiphoton scenario of the dissociative ATDI of H_2. The multicycle PS laser pulse with rotating polarization as a function of time has great potential to clock the ultrafast dynamics of molecules in strong laser fields.

This work was supported by the National Key R&D Program of China (Grant No. 2018YFA0306303), the National Natural Science Fund (Grants No. 11834004, No. 61690224, No. 11621404, No. 11704124, and No. 11761141004), the 111 project of China (Grant No. B12024), and Projects from Shanghai Science and Technology Commission (Grants No. 19JC1412200 and No. 19ZR1473900).

*jwu@phy.ecnu.edu.cn

[1] X. Gong, Q. Song, Q. Ji, K. Lin, H. Pan, J. Ding, H. Zeng, and J. Wu, Phys. Rev. Lett. **114**, 163001 (2015).
[2] P. Lu, W. Zhang, X. Gong, Q. Song, K. Lin, Q. Ji, J. Ma, F. He, H. Zeng, and J. Wu, Phys. Rev. A **95**, 033404 (2017).
[3] M. Lein, E. K. U. Gross, and V. Engel, Phys. Rev. A **64**, 023406 (2001).
[4] J. S. Parker, B. J. S. Doherty, K. T. Taylor, K. D. Schultz, C. I. Blaga, and L. F. DiMauro, Phys. Rev. Lett. **96**, 133001 (2006).
[5] Q. Liao and P. Lu, Phys. Rev. A **82**, 021403(R) (2010).
[6] G. S. J. Armstrong, J. S. Parker, and K. T. Taylor, New J. Phys. **13**, 013024 (2011).
[7] K. Henrichs, M. Waitz, F. Trinter, H. Kim, A. Menssen, H. Gassert, H. Sann, T. Jahnke, J. Wu, M. Pitzer, M. Richter, M. S. Schöffler, M. Kunitski, and R. Dörner, Phys. Rev. Lett. **111**, 113003 (2013).
[8] T. Seideman, M. Y. Ivanov, and P. B. Corkum, Phys. Rev. Lett. **75**, 2819 (1995).
[9] T. Zuo and A. D. Bandrauk, Phys. Rev. A **52**, R2511(R) (1995).
[10] B. D. Esry, A. M. Sayler, P. Q. Wang, K. D. Carnes, and I. Ben-Itzhak, Phys. Rev. Lett. **97**, 013003 (2006).
[11] C. B. Madsen, F. Anis, L. B. Madsen, and B. D. Esry, Phys. Rev. Lett. **109**, 163003 (2012).
[12] B. D. Esry and I. Ben-Itzhak, Phys. Rev. A **82**, 043409 (2010).
[13] P. Eckle, A. N. Pfeiffer, C. Cirelli, A. Staudte, R. Dörner, H. G. Muller, M. Büttiker, and U. Keller, Science **322**, 1525 (2008).
[14] P. Eckle, M. Smolarski, P. Schlup, J. Biegert, A. Staudte, M. Schöffler, H. G. Muller, R. Dörner, and U. Keller, Nat. Phys. **4**, 565 (2008).
[15] A. N. Pfeiffer, C. Cirelli, M. Smolarski, D. Dimitrovski, M. Abu-samha, L. B. Madsen, and U. Keller, Nat. Phys. **8**, 76 (2012).
[16] L. Holmegaard, J. L. Hansen, L. Kalhøj, S. L. Kragh, H. Stapelfeldt, F. Filsinger, J. Küpper, G. Meijer, D. Dimitrovski, M. Abu-samha, C. P. J. Martiny, and L. B. Madsen, Nat. Phys. **6**, 428 (2010).
[17] J. Wu, M. Meckel, L. Ph. H. Schmidt, M. Kunitski, S. Voss, H. Sann, H. Kim, T. Jahnke, A. Czasch, and R. Dörner, Nat. Commun. **3**, 1113 (2012).
[18] Q. Ji, S. Pan, P. He, J. Wang, P. Lu, H. Li, X. Gong, K. Lin, W. Zhang, J. Ma, H. Li, C. Duan, P. Liu, Y. Bai, R. Li, F. He, and J. Wu, Phys. Rev. Lett. **123**, 233202 (2019).
[19] G. Karras, M. Ndong, E. Hertz, D. Sugny, F. Billard, B. Lavorel, and O. Faucher, Phys. Rev. Lett. **114**, 103001 (2015).
[20] J. Ullrich, R. Moshammer, A. Dorn, R. Dörner, L. P. H. Schmidt, and H. Schmidt-Böcking, Rep. Prog. Phys. **66**, 1463 (2003).
[21] R. Dörner, V. Mergel, O. Jagutzki, L. Spielberger, J. Ullrich, R. Moshammer, and H. Schmidt-Böcking, Phys. Rep. **330**, 95 (2000).
[22] T.-Y. Xu and F. He, Phys. Rev. A **88**, 043426 (2013).
[23] J. Wu, M. Magrakvelidze, L. P. H. Schmidt, M. Kunitski, T. Pfeifer, M. Schöffler, M. Pitzer, M. Richter, S. Voss, H. Sann, H. Kim, J. Lower, T. Jahnke, A. Czasch, U. Thumm, and R. Dörner, Nat. Commun. **4**, 2177 (2013).
[24] Y. Mi, P. Peng, N. Camus, X. Sun, P. Fross, D. Martinez, Z. Dube, P. B. Corkum, D. M. Villeneuve, A. Staudte, R. Moshammer, and T. Pfeifer, Phys. Rev. Lett. **125**, 173201 (2020).